OpenNano 13 (2023) 100180

Contents lists available at ScienceDirect

OpenNano

journal homepage: www.elsevier.com/locate/onano

Pulmonary delivery of siRNA-loaded lipid-polymer hybrid nanoparticles: Effect of nanoparticle size

Abishek Wadhwa [a,1,3], Thomas R. Bobak [a,b,3], Lennart Bohrmann [b], Reka Geczy [a,b,2], Sathiya Sekar [b], Gowtham Sathyanarayanan [a], Jörg P. Kutter [a], Henrik Franzyk [c], Camilla Foged [a], Katayoun Saatchi [b], Urs O. Häfeli [a,b,*]

[a] Department of Pharmacy, Faculty of Health and Medical Sciences, University of Copenhagen, 2100 Copenhagen, Denmark
[b] Faculty of Pharmaceutical Sciences, University of British Columbia, Vancouver, BC V6T 1Z3, Canada
[c] Department of Drug Design and Pharmacology, Faculty of Health and Medical Sciences, University of Copenhagen, 2100 Copenhagen, Denmark

ARTICLE INFO

Keywords:
Microfluidics
siRNA
Lipid-polymer hybrid nanoparticles (LPNs)
Size modulation
SPECT/CT
Pulmonary delivery
Biodistribution

ABSTRACT

Nanomedicines based on nanoparticles rely both on the potency of the drug as well as the efficiency of the delivery system, for which particle size plays a crucial role. For the intracellular delivery of small interference RNA (siRNA), lipid-polymer nanoparticle (LPN) hybrid systems constitute a safe and highly effective class of delivery systems. In the present study, we employ a microfluidics method for the manufacturing of spherical siRNA-loaded LPNs for pulmonary delivery with distinct size distributions with average diameters of approximately 70, 110, and 220 nm. We designed an optically clear, inexpensive thiol-ene polymeric microfluidic chip prototype that is compatible with standard 'soft-lithography' techniques, allows for replica molding, and is resistant to harsh solvents. By using SPECT/CT in vivo imaging, we show comparable pulmonary clearance patterns of all three differently sized LPN formulations following intratracheal administration. Also, negligible accumulation in the liver was observed.

1. Background

RNA interference (RNAi)-based therapeutics can be a powerful tool in disease prevention and therapy [1]. RNAi is mediated by small interfering RNA (siRNA), and it provides highly specific and potent gene silencing. To be clinically effective, siRNA-based drug substances rely heavily on the delivery system. Nanoparticles (NPs) represent a highly desirable class of delivery systems due to their ability to protect siRNA against degradation by nucleases, as well as to modulate biodistribution and facilitate cellular uptake, endosomal escape, and delivery of siRNA to RNAi pathway in the cytosol [2]. An emerging class of promising NPs are lipid-polymer hybrid systems (LPNs), which combine the advantages of lipid- and polymer-based systems, i.e., the high siRNA loading and transfection efficiency of lipid-based systems and the higher structural integrity and colloidal stability of polymeric systems [3].

Previously, our group designed a highly effective LPN system for intracellular delivery of siRNAs [4]; showing high efficacy and low

* Corresponding author at: Faculty of Pharmaceutical Sciences, University of British Columbia, Vancouver, BC V6T 1Z3, Canada.
E-mail address: urs.hafeli@ubc.ca (U.O. Häfeli).
[1] *Current address:* Department of Microbiology and Immunology, University of British Columbia, Vancouver, BC Y6T 1Z3, Canada.
[2] *Current address:* Precision NanoSystems, Vancouver, BC V6P 6T7, Canada.
[3] These authors contributed equally.

https://doi.org/10.1016/j.onano.2023.100180
Received 31 December 2022; Received in revised form 16 April 2023; Accepted 31 July 2023
Available online 2 August 2023

toxicity for siRNA-mediated gene silencing as compared to existing formulations [5,6]. These LPNs are composed of the ionizable lipid-like (lipidoid) compound L_5N_{12} (Supplementary Material, Fig. S1) and the biodegradable and biocompatible polymer poly (DL-lactic-*co*-glycolic acid) (PLGA). For this system, we replaced cationic lipids (e.g., DOTAP) with lipidoid L_5N_{12} in order to reduce excessive surface charge and to increase the safety (reduce the toxicity) of the lipid nanoparticle system. This is attributed to the presence of several secondary and tertiary amines, rendering them more efficient in interacting with siRNA without significantly increasing the net charge of the delivery system [4]. Lipidoids offer a number of advantages, such as orders of magnitude lower siRNA dose requirements [7], lack of a permanent positive charge, and lower pKa values, which make them less likely to confer reactive oxygen species (ROS)-mediated toxicity [8,9]. Our recent studies suggest that siRNA-loaded LPNs display a core-shell structure, wherein the polymeric core functions as a colloid matrix support for siRNA-loaded lipidoid shell layers [10]. Furthermore, the incorporation of PLGA polymer has been demonstrated to enhance lung retention of siRNA when compared to its non-polymer counterpart (i.e., lipoplexes) [11] and confer sustained release properties to the nanoparticles [12].

The pulmonary route of administration is preferred for drugs used to treat obstructive airway diseases, e.g., chronic obstructive pulmonary disease (COPD) [13] and asthma. Avoidance of first-pass metabolism, reduction in therapeutic dose, and prevention of systemic side effects are some of the many advantages of local pulmonary delivery. Thus, targeting the pro-inflammatory cytokine tumor necrosis factor-α (TNF-α) with siRNA encapsulated in LPNs constitutes a promising approach for the reduction of chronic inflammation which is generally characteristic for obstructive airway diseases [11].

To optimize the dose fraction of siRNA that reaches the inflammatory cells in the lungs and to maximize cellular uptake, the LPN size is crucial, and several reports have demonstrated that a diameter range of 50 to 100 nm is desirable for optimal tissue penetration upon systemic administration [14–16]. Furthermore, NP size has been reported to determine the cellular uptake pathway, where endosomal uptake is minimal for spherical sizes of 50 to 100 nm, thereby leading to a most favorable cell uptake [17–19]. However, to achieve nanoparticle size distributions in these ranges, traditional NP fabrication methods, such as the double emulsion solvent evaporation (DESE) method, fall short in enabling a high degree of size modulation. To obtain specific NP size and narrow size distributions, we focused on the use of novel microfluidic fabrication approaches.

Microfluidics has the potential to produce drug carriers with tunable size characteristics, high drug encapsulation efficiency and loading, narrow particle size distribution, and the elimination or minimization of post-production procedures such as purification and size adjustment [20]. Through microfluidics, siRNA-loaded lipid [21–23] and unloaded lipid-polymer [24–26] nanoparticles can be tailored as small as 30 nm in diameter. The smallest siRNA-containing LPNs have been reported to be 110–130 nm in diameter [27,28]. Microfluidic methods generally rely on one-step nanoprecipitation [29], where rapid mixing results in solvent displacement, thereby leading to self-assembly of the polymer and lipid into nanoparticles. Here, the mixing rate is critical, though other formulation parameters e.g., the solute concentration and the solvent polarity, are also affecting the final nanoparticle size [30].

A final consideration for a microfluidic set up is the device material used to manufacture the mixer. Polydimethylsiloxane (PDMS) is by far the most commonly used material in an academic setting due to its ease of fabrication through replica molding [31]. This study focuses on the use of a thiol-ene (TE) polymer that shows great promise as an inexpensive and easy to produce alternative to PDMS. This material displays superior chemical compatibility with most organic solvents [32], while being rigid, which allows for manufacturing with high flow rates (and consequently high pressure) [33]. Also, this material provides low small-molecule permeability [34], and thus possesses features particularly suited for the production of LPNs.

Previously, we investigated the effect of formulation parameters on lung retention upon pulmonary administration of siRNA-loaded LPNs [11]. However, due to the limitations of the traditional fabrication, such as the DESE method, a systematic study to investigate the impact of size modulation could not be done. Therefore, the present investigation aimed to produce size-modulated LPNs using microfluidics by utilizing a novel TE-microfluidic chip design, and to investigate the biodistribution of differently sized LPNs by SPECT/CT imaging in vivo following intratracheal administration to improve the understanding of pulmonary NP uptake/clearance with organ resolution. Hitherto, no studies concerning TE-microfluidic production of siRNA-loaded LPNs with tunable size have been reported. The LPNs were imaged by incorporation of the lipid chelator phosphoethanolamine diethylenetriaminepentaacetic acid (PE-DTPA), which was radiolabeled with the γ-emitting isotope ^{111}In ($T_{1/2} = 67.2$ h, Eγ = 171 and 245 keV). We hypothesized that the size of LPNs impact pulmonary distribution/retention and elimination of siRNA-loaded LPNs. It was furthermore hypothesized that low or negligible liver uptake of all NP sizes would occur following pulmonary administration.

2. Materials and methods

2.1. Materials

L_5N_{12} was synthesized, purified, and characterized as reported earlier [4]. 2′-*O*-Methyl-modified dicer substrate asymmetric siRNA duplex directed against TNF-α (17,928.33 g/mol) was synthesized, purified, and kindly provided by GlaxoSmithKline (Stevenage, UK) as a dried, purified, and desalted duplex. The siRNA had the following sequence and modification pattern: Guide/antisense strand: 5′-AGCAGGAAUGAGAAGAGGCUGAGACAU-3′, and passenger/sense strand: 5′-pGUCUCAGCCUCUUCUCAUUCCUGct-3′, where upper case letters are ribonucleotides, lower case letters represent deoxyribonucleotides, underlined capital letters are 2′-*O*-methylribonucleotides, and p denotes a phosphate residue. Ester-terminated PLGA (lactide:glycolide molar ratio 75:25, M_w 20 kDa) was acquired from Evonik Industries (Essen, Germany). PE-DTPA was procured from Avanti Polar Lipids (Alabaster, AL, USA). Quant-iT□ RiboGreen□ RNA reagent and Tris-EDTA (10 mM Tris, 1 mM, EDTA pH = 8.0) were from Molecular Probes Invitrogen (Paisley, UK). Heparin sodium salt, sodium acetate trihydrate, HPLC-grade acetone, and diethyl pyrocarbonate (DEPC) were from Sigma Aldrich (St. Louis, MO, USA). Glacial acetic acid was from Alfa Aesar (Tewksbury, MA, USA), and absolute ethanol was from Commercial Alcohols

(Brampton, ON, Canada). The Sylgard 184-poly(dimethyl siloxane) (PDMS) elastomer kit was acquired from Dow Corning (Midland, MI, USA). Pentaerythritol tetrakis (3-mercaptopropionate) and triallyl-1,3,5-triazine-2,4,6- (1H, 3H, 5H)-trione was from Sigma Aldrich (Brøndby, Denmark).

2.2. Microfluidic chip fabrication

Thiol-ene chips were fabricated as described previously [35]. Master molds were fabricated by milling PMMA plates using a computer-numerated control (CNC) mill, MiniMill (Minitech Machinery, Norcross, GA, USA), and spacers and lids were CO_2 laser cut using Epilog Laser Mini 18 (Golden, CO, USA). PDMS was casted into the cavity formed by the master mold, spacer, and lid, and cured for 2 h at 80 °C. Stoichiometric thiol-ene was molded within the PDMS negatives, at a stochiometric ratio of 1.60 using the monomers 1,3,5-triallyl-1,3,5-triazine-2,4,6(1H,3H,5H)-trione and pentaerythritol tetrakis(3-mercaptopropionate), respectively (both from Sigma Aldrich, Schnelldorf, Germany). The monomer mixture contained 1% of the photoinitiator Lucirin□ TPO-L (BASF, Ludwigshafen, Germany). Nonbonding sides of the molds were exposed to 2.0 s UV light (12 mW/cm^2 at 365 nm) using an LS-100-3C2 near UV light source (Bachur & Associates, Santa Clara, CA, USA), and the chips were assembled by manually pressing the two halves together. The chips were exposed to high-intensity UV light for a final cure, 10 min exposure of each face (90 mW/cm^2 at 365 nm) using a Dymax 5000-EC Series UV curing flood lamp (Dymax Corp., Torrington, CT, USA). The TE-microfluidic chip had a length of 22 mm, a width of 15 mm and a height of 4 mm. The chip design was drawn using a combination of Autodesk□ Inventor□ Professional (Autodesk, San Rafael, CA, USA) and the CNC mill programmed using InventorCAM (SolidCAM, Newtown, PA, USA).

2.3. Microfluidic chip design

A two-inlet flow-focusing geometry was combined with a novel "split-and-recombine" mixing region (Fig. S2) that was experimentally prototyped to yield distinct LPN sizes primary by varying the total flow rate (TFR). For size modulation, the most effective chip geometry consisted of five "split-and-recombine" mixing regions that create points of constrictions and expansions by varying depths and widths. The primary depth of the microfluidic channels was held at 125 μm, but included 10 deepened channels in the mixing region, which were 300 μm deep. Similarly, the channel widths of the mixing region were varied between 150 and 400 μm to further create points of constrictions and expansions. Additional sharp corners were maintained to further enhance chaotic advection in the region. Finally, the main inlet and outlet channel widths were 500 μm wide × 125 μm deep and spaced 3 mm apart to fit a commercial manifold, Interface H and 4 Linear Connector 4-way system (Dolomite, Royston, UK).

2.4. Thiol-ene microfluidic production of lipid-polymer hybrid nanoparticles

The TE-microfluidic chip was connected to gas-tight syringes (Hamilton, Reno, NV, USA) using 0.5 mm inner diameter poly-(tetrafluoroethylene) (PTFE) tubing, in-house fabricated PDMS O-rings, and a four-inlet H interface (Dolomite). A 2.5 mL syringe and a 1 mL syringe were used to load the water phase and organic phase, respectively. The water phase consisted of a solution of siRNA (25 μg/mL) in sodium acetate buffer (125 mM, pH 5.2) prepared using filtered DEPC treated water for (final volume of 1.5 mL per batch). The organic phase consisted of L_5N_{12} (1.125 mg/mL) and PLGA (6.375 mg/mL) dissolved in acidified acetone (14 μL glacial acetic acid per mL acetone) to a final volume of 0.5 mL per batch. Hence, the L_5N_{12} content relative to the total solid content (L_5N_{12} and PLGA) was 15% (w/w) and the L_5N_{12}:TNF-α siRNA ratio was 15:1 (w/w), as previously optimized [36].

The two phases were pumped into the TE-microfluidic chip at room temperature (RT) using Fusion 200 syringe pumps (Chemyx; Stafford, TX, USA), which were adjusted for the specific syringe. The chip was kept in place using a custom-made plastic chip holder. The water phase and the organic phase were mixed at a FFR of 3:1 (water:org) at different TFRs of 3.4 and 4 mL/min for the production of LPNs, which displayed mean diameters of approximately 220 nm and 110 nm, respectively (referred to as 200 nm LPNs and 100 nm LPNs below). A FFR of 2.6:1 (water:org) at a TFR of 5.8 mL/min was used for production of LPNs, which had a mean diameter of approximately 70 nm (referred to as 70 nm LPNs below). The initial 0.15 mL and the last 0.05 mL of the resulting LPN dispersion were discarded, while the remaining volume was collected as the sample fraction. An inverted microscope was used to visually inspect the mixing channels before LPN preparation and to ensure that no bubbles were present during LPN production. Chips were typically rinsed and re-used for approximately 10 batches of LPNs if they appeared intact upon proper evaluation under a microscope and verification of retained flow properties. Final purification and removal of un-encapsulated siRNA, chelator, and organic solvents was performed by membrane-embedded centrifugal filtration using filters with a MW cut-off of 100 kDa (Amicon Ultra-0.5–100 kDa, Sigma-Aldrich). Due to the chemical incompatibility between acetone and the centrifugal filter, the organic solvent was evaporated prior to filtration by assisted airflow. Three-time centrifuge-assisted dialysis was performed with 100 kDa Amicon filters at 4 °C for 10 min at 4.000 rpm by mixing 100 μL LPN with 400 μL DEPC treated water. Subsequently, the supernatant was spun down by turning the filter upside down and centrifuging at 4 °C for 5 min at 5000 rpm. The collected volume (~50 μL) was adjusted with water to a final volume of 100 μL.

2.5. Physicochemical characterization

Dynamic light scattering was used to determine the hydrodynamic diameter (z-average) and polydispersity index (PDI) of the nanoparticle dispersions using a Zetasizer (Malvern Instruments, Worcestershire, UK), while the zeta potential and the siRNA encapsulation efficiency were determined by using laser Doppler microelectrophoresis and the Quant-iT□ Ribogreen□ RNA reagent

(fluorescence spectroscopy), respectively, as reported previously [37].

2.6. Cryogenic transmission electron microscopy (Cryo-TEM)

Morphological analysis was carried out by cryogenic transmission electron microscopy (cryo-TEM) using a Tecnai G2 20 TWIN transmission electron microscope (FEI, Hillsboro, OR, USA). Samples for cryo-TEM were prepared using a FEI Vitrobot Mark IV (Thermo Fischer Scientific, Waltham MA, USA), under controlled temperature and humidity conditions within an environmental vitrification system. A 2 μL droplet was deposited onto a Pelco Lacey carbon-filmed grid and spread carefully. Excess liquid was removed resulting in the formation of a thin (10–500 nm) sample film. The samples were immediately plunged into liquid ethane and kept at −180 °C for vitrification. The vitrified samples were subsequently transferred in liquid nitrogen to an Oxford CT3500 cryo holder connected to the electron microscope. The sample temperature was continuously kept below −180 °C. All observations were made in the bright field mode at an acceleration voltage of 120 kV. Digital images were recorded with a Gatan Imaging Filter 100 CCD camera (Gatan, Pleasanton, CA, USA).

2.7. Radiolabeling of LPNs

The radiolabeling of the LPNs with ^{111}In was performed by dissolving 18:0 PE-DTPA in absolute ethanol at 0.4 mg/mL by incubation in a 50 °C water bath for 2 h for complete solubilization. Subsequently, the glass vial was cooled to RT before addition of 5 mol. % L_5N_{12} to the organic phase. The PE-DTPA-containing LPNs were produced by TE-microfluidics as described in Section 2.4. After purification, 37–74 megabecquerel (MBq) of $^{111}InCl_3$ (0.5–6.0 μL volume, according to activity) in 0.1 M HCl was added to 100 μL PE-DTPA-containing LPN suspension and incubated at RT for 1 h in a Thermomixer R (Eppendorf, Mississauga, ON, Canada) shaking at 400 rpm prior to instant thin layer chromatography (ITLC) evaluation. Here, the ITLC (Tec-Control□, #151-005, Biodex Medical systems) was used with 0.1 mM EDTA as the mobile phase. In this system, free ^{111}In complexed with EDTA migrates to $R_f = 1$ while ^{111}In-LPNs remain at $R_f = 0$ (Fig. S3) The ITLCs were visualized using a phosphor imager (Cyclone, Canberra Packard, Mississauga, CA) and quantified with the OptiQuant software (Perkin Elmer). If the radiochemical efficiency was below 95%, three washing steps with 400 μL DEPC water were performed by using a protocol similar to that described in Section 2.4.

2.8. Evaluation of the pharmacokinetics and biodistribution of LPNs using SPECT/CT

The pharmacokinetics and biodistribution of LPN formulations were evaluated quantitively by radiolabeling the LPN formulations with ^{111}In. All formulations were prepared one day before radiolabeling and administered on the following day. The clearance patterns of the three LPN formulations following intratracheal administrations were detected by single photon emission computed tomography / computed tomography (SPECT/CT). The imaging studies were performed in accordance with the Canadian Council on Animal Care (CCAC), and the protocols were approved by the Animal Care Committee (ACC) of the University of British Columbia (A20-0132). Female C57BL/6 mice (18 weeks old) were acquired from Charles River Laboratories (Wilmington, MA) and acclimatized for one week before experimental manipulation. Mice were allocated into groups of four individuals and anesthetized by isoflurane inhalation. The mice were dosed by intratracheal administration with 25 μL of ^{111}In-LPNs containing 3.7–5.9 MBq of ^{111}In and ~30 μg L_5N_{12} each. Due to misadministration, the 220 nm group only contained three animals (Fig. S4). At 0, 4, and 24 h after administration, SPECT/CT scans were performed using a VECTor/CT preclinical small animal scanner (MILabs, Utrecht, The Netherlands). The details of SPECT/CT scanning and reconstruction are provided (Supplementary Materials 5.) The radioactivity in the lungs, trachea and mouth, bladder, and stomach were quantified by drawing 3D volumes of interest (VOIs) using Amide software V.1.0.4 [38]. The decay corrected remaining percentage of injected dose per organ at each time point was plotted as a function of the time to compare the pulmonary clearance of the three LPN formulations. After the final SPECT/CT scans at 24 h post injection, the animals were euthanized, and their blood, heart, liver, kidneys, lungs, small intestine, brain, bladder, muscle, spleen, bone, pancreas, feces, and stomach were collected, cleaned and weighed. The radioactivity in each organ was measured using a gamma counter (Packard Cobra II Autogamma counter, PerkinElmer).

2.9. Statistics

Results are expressed as mean values ± standard deviation (SD). The obtained responses were subsequently subjected to ANOVA, followed by a Dunnett's multiple comparison test as recommended by GraphPad Prism (version 8.0, GraphPad Software, La Jolla, CA, USA). The significance of the results is indicated according to p-values (* $p < 0.05$; ** $p < 0.01$; *** $p < 0.001$; and **** $p < 0.0001$). A p-value below 0.05 was considered statistically significant.

3. Results and discussion

3.1. Thiol-ene microfluidic production of LPNs and physicochemical characterization

The previously optimized the L_5N_{12}-modified LPN delivery system, which demonstrated high efficacy and low toxicity for siRNA-mediated gene silencing as compared to existing formulations, was produced by using a DESE method [4,12]. Using this preparation method results in an effective delivery system for siRNA encapsulation and transfection efficiency, but this batch method does not

allow for controllable particle size design, consistently yielding NPs with diameters in the range of 170–220 nm.

In order to manufacture LPNs with controllable particle size, LPNs were formed through nanoprecipitation of the dissolved solids within organic and aqueous phases using a TE-microfluidic chip. Based on computational fluid dynamics (CFD), square mixing chambers have been found to exhibit better mixing performance than micromixers with circular chambers [39]. The microfluidic chip geometry and LPN formation are illustrated in Fig. 1A. The concentration of leachables and extractables decrease with increasing degree of crosslinking of the polymer. Therefore, the monomer and photoinitiator concentrations were optimized for the highest crosslinking, solvent resistance, and robustness of the thiol-ene polymer (Fig S5).

The two phases containing the dissolved constituents are introduced into the channels and flow-focused into a mixing region with five consecutive squares-like mixing chambers. This mixing region contains abrupt flow path shifts, constrictions, and expansions (achieved through variable depths and widths), ultimately leading to vortex formation to mix the solutions. Estimates of the Reynolds numbers for the three differently sized LPN formulations all indicate laminar flow (i.e., Re $<$ 2000, Table S1).

To achieve faster mixing and smaller LPN size, the squares-like elements combined with the increased flow rates allow for higher chaotic advection through the bulk motion of the fluids (i.e., resulting in higher Peclét numbers). Homogenous mixing is rapidly achieved as the organic/aqueous phases pass through the mixing region, resulting in formation of uniform LPNs (Fig. 1B)

To control the LPN size, the microfluidic nanoprecipitation process parameters (TFR and FRR) were explored. Modulating the process parameters allowed us to design three differently sized siRNA-loaded LPN formulations with average diameters of approximately 79 nm, 112 nm, and 227 nm, respectively (for the sake of clarity referred to as 70 nm, 110 nm and 220 nm LPNs below), with relatively narrow size distributions (Fig. 2A/B and Table S2.). The smallest 70 nm LPNs were produced at the highest possible TFR of 5.8 mL/min and an FFR of 2.6:1, whereas TFRs of 4.0 mL/min and 3.4 mL/min and an FFR of 3:1 were applied to manufacture the 110 nm and 220 nm siRNA-loaded LPNs, respectively. A significant ($p < 0.0001$) increase in the zeta potential from approximately 30 mV to 55 mV (Fig. 2C and Table S2) was observed when the LPN size was increased from 70 nm to 220 nm, probably due to the larger surface area of the 220 nm LPNs. The siRNA encapsulation efficiencies of the siRNA-loaded LPNs were found to be 70 $\pm$ 7%, 43 $\pm$ 10%, and 49.8 $\pm$ 1.3% for the 70 nm, 110 nm, and 220 nm LPNs, respectively, as reported previously for LPNs using other manufacturing methods [37]. It has been reported in the literature that with the increasing particle sizes obtained at low flow rates in the downstream flow, the lipid components may experience suboptimal environments in the mixing equipment that may lead to precipitation [5]. This may explain the lower siRNA encapsulation measured for the larger-sized (110 and 220 nm) LPNs.

Further size modulation can be achieved by adjusting the solvent polarity. The polarity of the organic phase affects the resulting LPN size due to diffusion modulation, i.e., the more polar the lipid solvent is, the faster it diffuses into the water phase, yielding NPs with smaller sizes. Previously, 95% acetone has been used for batch nanoprecipitation of siRNA-loaded LPNs, providing excellent chemical siRNA stability in that solvent [40]. Most microfluidic mixing processes for preparation of lipid-based nanoparticles involve the use of ethanol as the organic solvent with a buffered aqueous phase, because most microfluidic chips are not compatible with the use of acetone as a solvent [20]. However, thiol-ene microfluidic chips are compatible with a wide variety of solvents, including harsher organic solvents, such as chloroform and acetone (Fig. S5), and hence enabling nanoparticle size modulation through adjustment of the organic solvent polarity.

The solvents used for the preparation of siRNA-loaded LPNs must be chosen based on the solubility of the lipids and the polymer. While PLGA can be dissolved in solvents like acetone, acetonitrile, anisole, chloroform, dichloromethane, dimethylformamide, dimethylsulfoxide (DMSO), ethyl acetate, and dioxane [41], the relevant solvent(s) constituting the organic phase must also be water-miscible, have chemical compatibility with plastics (e.g., the TE-microfluidic mixer and the ultrafiltration membrane), and

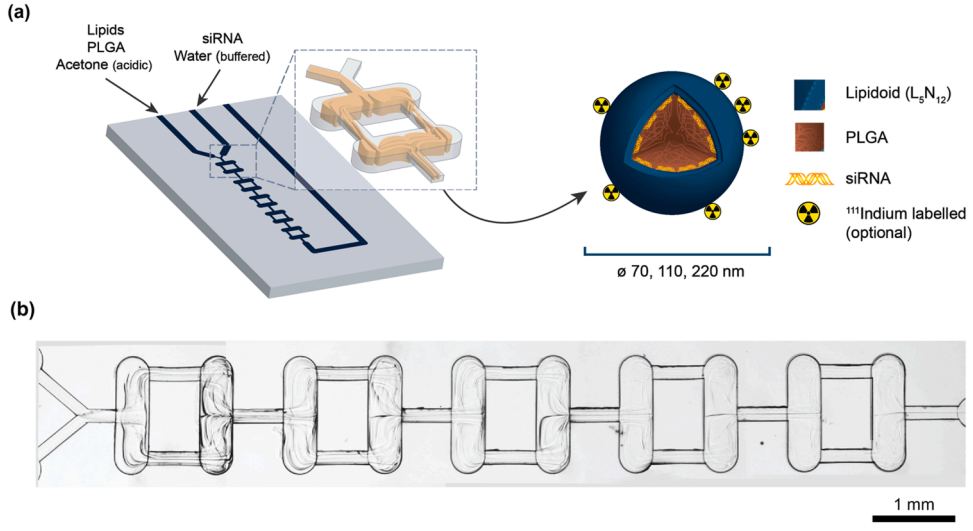

Fig. 1. (a) Illustration of the in-house designed and fabricated thiol-ene microfluidic chip and illustration of resulting LPNs and constituents. (b) Light microscopy image of LPN production showing microfluidic mixing of the phases towards the 4th and 5th mixer repeat.

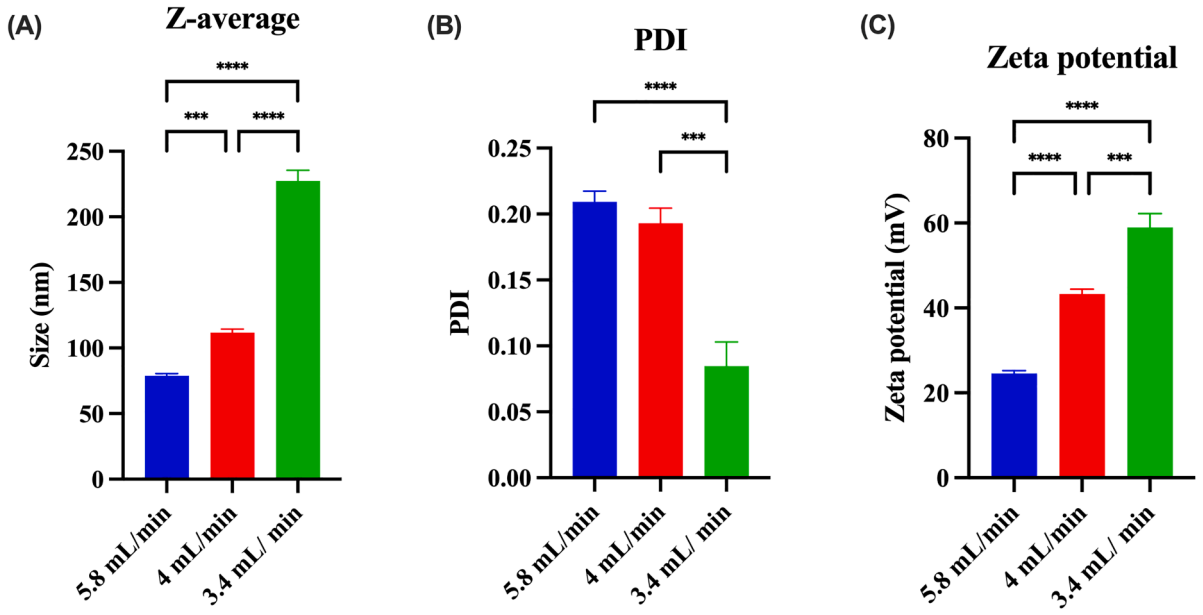

Fig. 2. (A) Size (z-average), (B) polydispersity index, and (C) zeta potential of the differently sized LPN formulations, produced at different total flow rates. Columns represent mean values ± SD. $n = 3$, $N = 3$. Statistically significant differences are indicated: $^{*}p < 0.05$, $^{**}p < 0.01$, $^{***}p < 0.001$, and $^{****}p < 0.0001$. Colour code: Blue: 70 nm LPNs, red: 110 nm LPNs, green: 220 nm LPNs. (For interpretation of the references to colour in this figure legend, the reader is referred to the web version of this article.)

preferably have a low boiling point to allow for downstream solvent evaporation [42]. Appropriate organic solvents for PLGA, based on solubility and water miscibility, are thus limited to acetone, acetonitrile, and DMSO. The latter may act as a free radical scavenger and is able to penetrate cell membranes thereby compromising the integrity of cell membranes [43]. Hence, DMSO is toxic, and as it is also challenging to ensure its complete removal due to its high boiling point, we did not consider it further. From the two remaining solvents, acetone is the best solvent for L_5N_{12} at low pH, likely due to a lower solvent polarity index for acetone (i.e., 5.1) in contrast to that of acetonitrile (5.8). At pH 7.4, ionizable lipids are mainly non-polar or only slightly polar, with very few charges. Acidification of the organic solvent leads to protonation of the lipid headgroups, hence facilitating solubilization. As revealed by the in silico studies, protonation of L_5N_{12} occurs at positions N2 and N4 at pH 7.0 and at N1, N2, and N4 under more acidic conditions at pH 6.0 [5]. Therefore, acetone acidified with glacial acetic acid was chosen as the organic solvent for formulation of the LPNs. As RNA is susceptible to alkaline hydrolysis at pH > 6, and to acidic hydrolysis at pH < 2 [44], we chose a sodium acetate buffer (125 mM, pH ~5.2), which has previously been employed for siRNA delivery with L_5N_{12} [45].

All LPN formulations consisted of spherical particles as shown using cryo-TEM (Fig. 3). The LPNs displayed an electron-dense core, corroborating the previously found core-shell structure of siRNA-loaded LPNs [10]. In addition, the structure of LPNs prepared using microfluidics resembled that of siRNA-loaded LPNs prepared by using the DESE method [4]. The broadness of the size distribution (measured as the PDI) of the LPN formulations prepared using the TE-microfluidic method were below 0.2 (Fig. 2), similar to the formulations prepared using the DESE method.

3.2. *Radiolabeling and SPECT/CT imaging of 70, 110, and 220 nm LPNs*

To allow for SPECT/CT imaging, a lipophilic chelator was incorporated into the LPNs during the microfluidic LPN preparation by dissolving it into the lipid phase. In this way, the lipid chelator with two saturated C18 stearoyl chains is expected to be incorporated into the LPN structure, which is hydrophobic, and hence the chelator will have a very high affinity for the LPNs. The addition of PE-

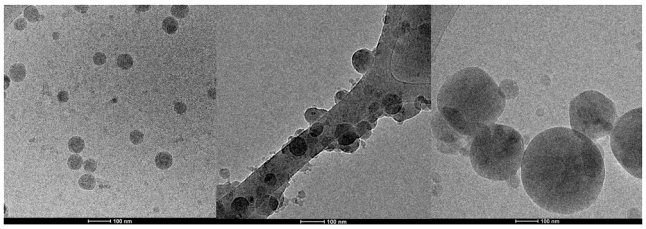

Fig. 3. Representative cryo-TEM images of LPN formulations with sizes of 70 nm, 110 nm, and 220 nm. All scale bars are 100 nm.

DTPA followed by radiolabeling with ^{111}In did not influence the physicochemical characteristics of the LPNs; importantly, the size remained comparable to that of the controls (Fig. S6). The radiolabeling efficiencies were 95% or higher for the LPNs used for the in vivo studies (Fig. S3). All formulations were administered into the trachea of the mice. The LPNs were homogenously distributed into the left and right lung lobes with residual LPNs located in the trachea and the mouth (Figs. 4–6). Overall, 70–90% of the dose of the three different size-modulated LPN formulations were deposited in the lungs following intratracheal administration (Fig. 7). After 24 h, 35 ± 7% of the injected dose of the 70 nm LPNs remained in the lungs, while the retention for the 110 nm LPNs and the 220 nm LPNs was found to lower with 26 ± 8% and 25 ± 11% of the injected dose, respectively, but this difference was not statistically significantly ($p > 0.05$).

We have previously studied the in vivo biodistribution for this delivery system (L_5N_{12}-modified LPNs) loaded with Alexa Fluor 750-labelled siRNA upon pulmonary administration in mice using quantitative fluorescence imaging tomography [11]. These studies showed that pulmonary administered siRNA-loaded LPNs display enhanced lung retention of siRNA, as compared to non-loaded siRNA, which suggests that formulation of siRNA into nanoparticles enhances the lung retention of siRNA. In addition, siRNA was permeating the air-blood barrier and was cleared from lung tissue after pulmonary administration, followed by excretion via the kidneys. The siRNA release profile from the optimized LPN formulation (i.e., a content of 15% L_5N_{12} and an L_5N_{12}:siRNA ratio of 15:1) displayed a cumulative release of 66% after 6 h, and therefore a timepoint of 24 h was considered appropriate for the present study.

The clearance rate of LPNs from the lungs has previously been shown to be much slower than the clearance rate of lipoplexes [46]. This observation was attributed to the sustained release characteristics of LPNs conferred by PLGA. The three differently sized LPN formulations investigated in the present study exhibited similar pulmonary clearance kinetics, which suggests comparable mucociliary clearance for LPNs with diameters in the range of 70–220 nm. A study supports these findings, demonstrating that mucociliary clearance of micro- and nano-meter sized particles is independent of size, shape, and charge [47]. Similar to our hypothesis, another study investigated solid lipid nanoparticles with a wider size range, and reported that larger sized particles (approx. 480 nm in diameter) display longer lung retention times than smaller sized particles (approx. 120 nm in diameter) [48]. We did not find any statistical significant difference in lung retention time at 24 h in the pharmacokinetic study between sizes for the LPN formulations that we chose to investigate, contrary to our hypothesis.

Another physicochemical property of the LPNs to consider is the surface charge, which is a defining factor for pulmonary delivery, because it influences the permeability through the surfactant layer and mucociliary – and macrophage clearance, among others [49]. We recently studied the interactions between siRNA-loaded LPNs and pulmonary surfactant [37]. We found that positively charged LPNs were capable of disrupting the pulmonary surfactant layer, and it is likely that the present three LPN formulations of different sizes affect the pulmonary surfactant layer to the same extent.

Between 9–23% of the injected LPN dose was present in the trachea at 0 h, which was transported via mucociliary clearance to the mouth of the animals and was subsequently swallowed and almost completely cleared after 24 h (Fig. 7). The successful intratracheal

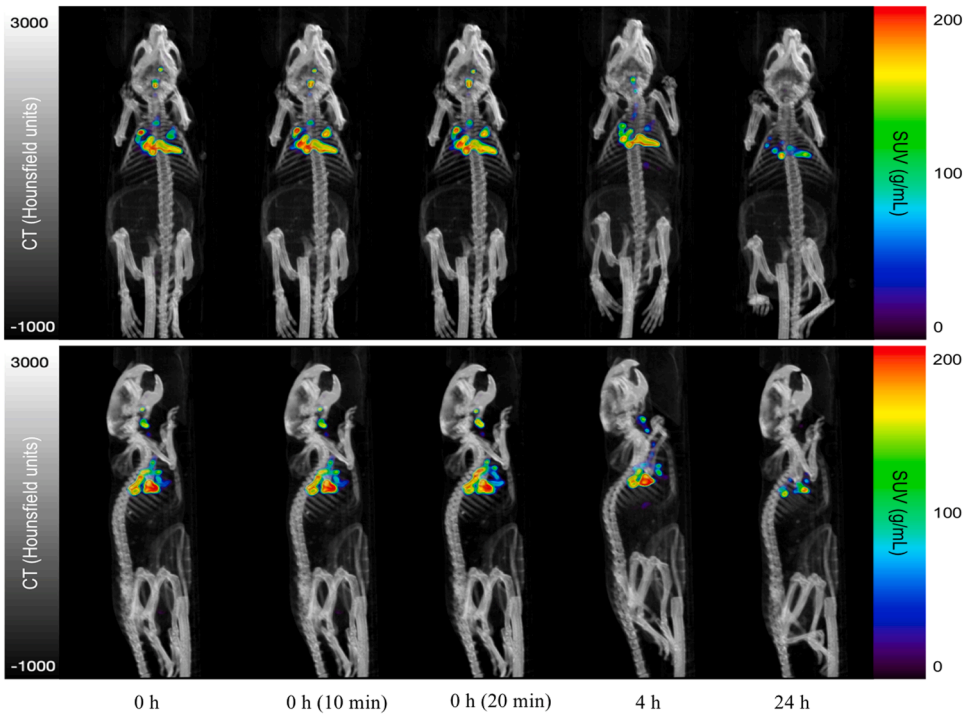

Fig. 4. Representative coronal (top) and sagittal (bottom) SPECT/CT images following intratracheal administration of 70 nm LPNs over time (0–24 h). Images indicate that LPNs in the upper airways are cleared faster than LPNs deposited in the lower airways (lungs). SUV: Standard uptake value.

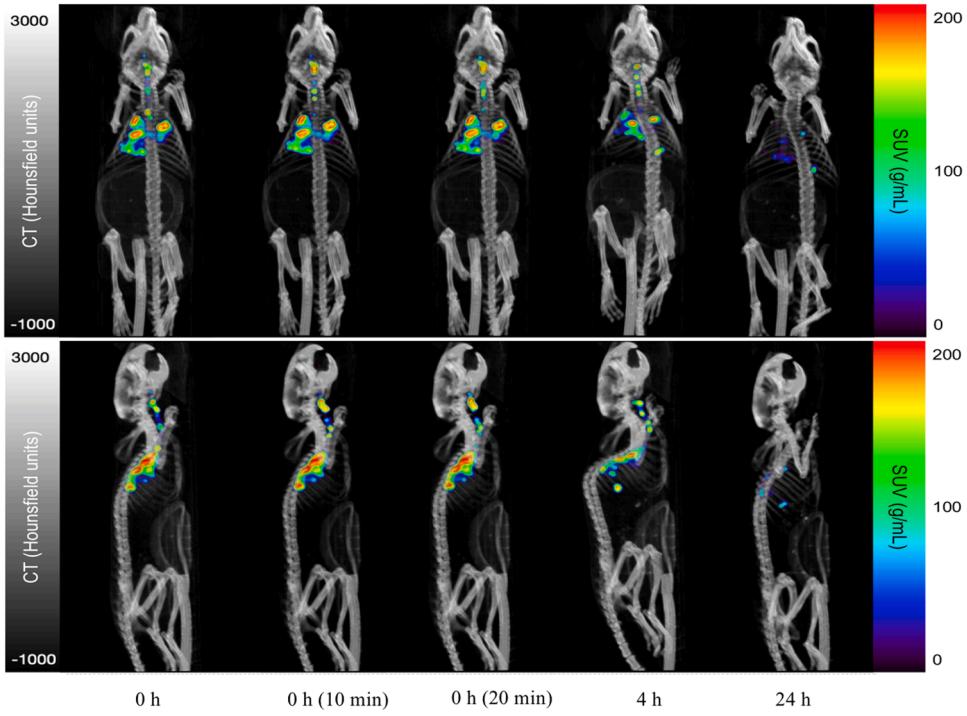

Fig. 5. Representative coronal (top) and sagittal (bottom) SPECT/CT images following intratracheal administration of 110 nm LPNs over time (0–24 h). SUV: Standard uptake value.

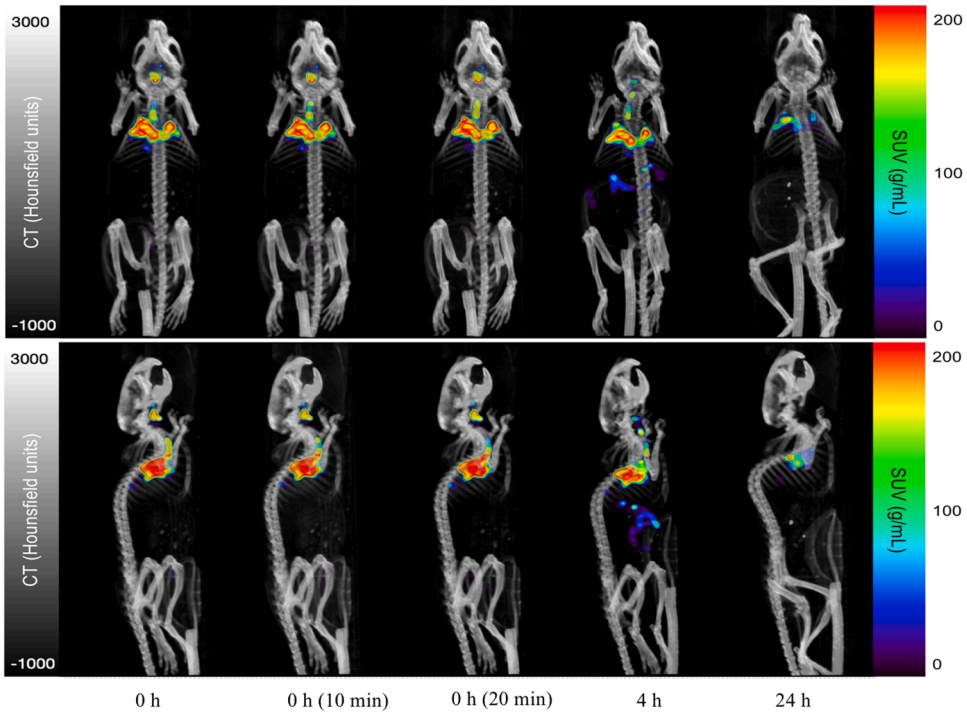

Fig. 6. Representative coronal (top) and sagittal (bottom) SPECT/CT images following intratracheal administration of 220 nm LPNs over time (0–24 h). SUV: Standard uptake value.

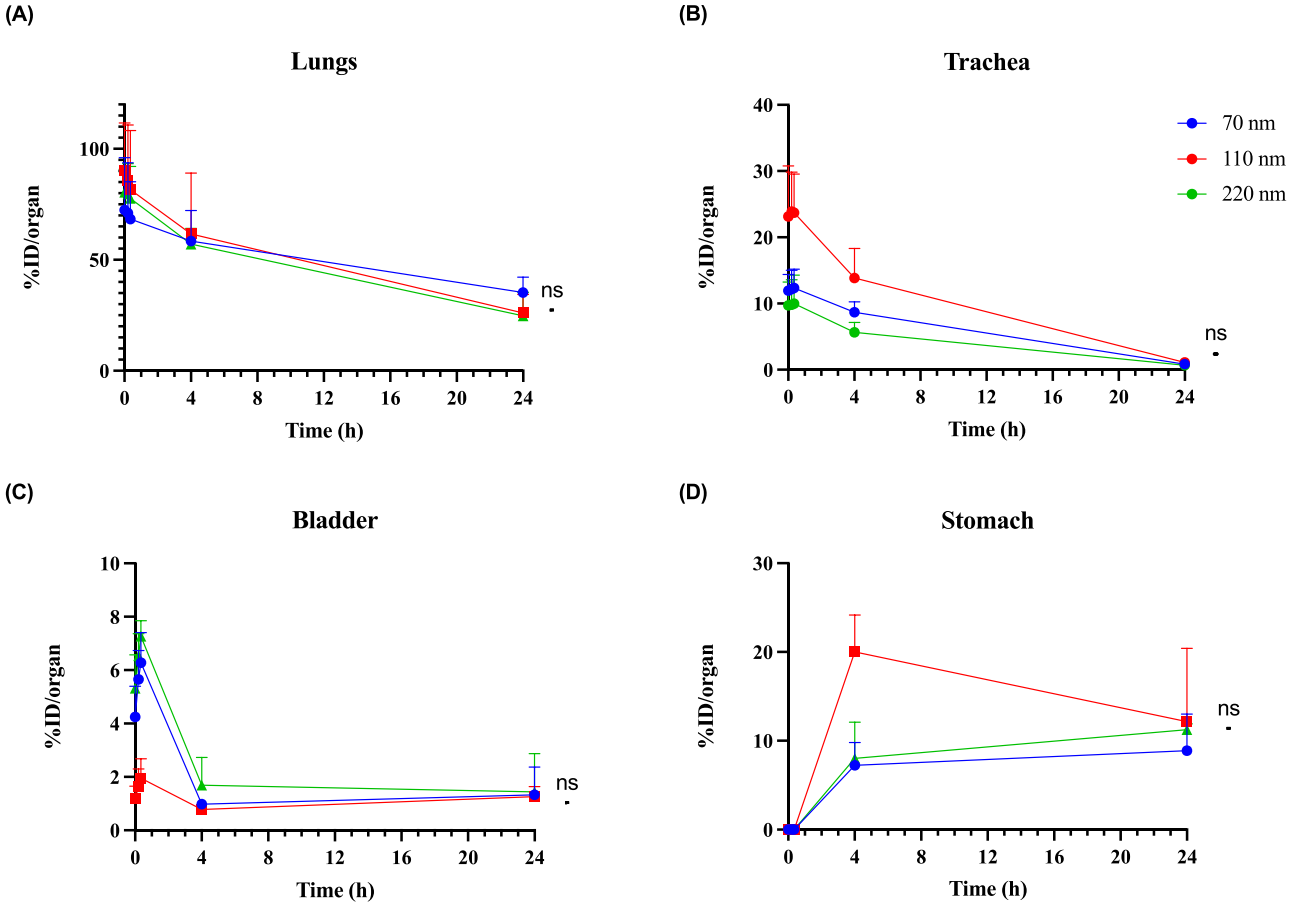

Fig. 7. Clearance pharmacokinetics of the three differently sized LPN formulations in (A) the lungs, (B) the trachea, (C) the bladder, and (D) the stomach, as obtained by image analysis of the SPECT/CT data. Data points represent mean values ± SD ($n = 4$). "ns" denotes statistical non-significance of the three formulations at the 24-h timepoint. Colour code: Blue: 70 nm LPNs, red: 110 nm LPNs, green: 220 nm LPNs. (For interpretation of the references to colour in this figure legend, the reader is referred to the web version of this article.)

administration is illustrated with no LPNs present in the stomach at 0 h. Swallowing of LPNs into the stomach and transit of the LPNs through the gastro-intestinal tract (GI-tract) appears constant between 4 h and 24 h. The radioactivity of LPNs in the bladder was reduced from 4.3 ± 1.2% to 1.3 ± 1.0%, from 1.2 ± 0.5% to 1.3 ± 0.4%, and from 5.3 ± 1.3% to 1.4 ± 1.4% for 70 nm, 110 nm, and 220 nm LPNs, respectively. The radioactivity in the bladders can be attributed to free isotope, i.e., $^{111}In^{3+}$.

3.3. Organ level biodistribution of 70, 110, and 220 nm LPNs

Scintillation counting was used to quantify the biodistribution at an organ level of the three differently sized LPN formulations since it has higher sensitivity than 3D imaging. Biodistribution data obtained after the last imaging time point at 24 h (Fig. 8) shows that a large fraction of the inhaled LPN formulations remained in the lungs with less than 3% of LPN formulations found in other organs. The presence of LPN formulations in the feces confirms mucociliary clearance and subsequent swallowing of the LPNs through the esophagus into the GI tract, which is reported to be the major clearance mechanism of the formulations deposited in the upper respiratory tract [46]. A statistically significant difference was seen between the lung content of 110 nm LPN formulation and the two other sized LPN formulations 24 h post administration. Further studies are needed to clarify whether the observed difference in lung content can be explained exclusively by differences in cellular uptake into alveolar macrophages and epithelial cells of the lungs. Difference in penetration of mucus or in initial deep lung deposition of the three differently sized LPN formulations might also influence the final lung content 24 h post administration.

Approximately 1% of the injected dose of the LPN formulations was found in the liver 24 h post administration, which infers that pulmonary delivery results in negligible liver accumulation, independent of LPN size within the range of 70–220 nm. In a previous study, the cholesterol analog β-sitosterol was incorporated into lipid nanoparticles to improve endosomal escape, while PEG-lipids were included for enhanced stability of lipid nanoparticles sized between 60 and 100 nm, which allowed for delivery of mRNA through inhalation [50]. Furthermore, gene expression of mRNA was only detected in the lungs following inhalation as administration route [50].

PLGA microspheres (mean diameter of 12 μm) have been designed for passive lung targeting following intravenous administration by alveolar capillary targeting [51]. Homogenous distribution in both lungs lobes was found, but biodistribution data of ^{111}In-DTPA PLGA 10 days post administration also showed the presence of ^{111}In-DTPA PLGA in the kidneys, the spleen, and the liver. Hence, local administration in the airways results in preferential LPN retention in the lung tissue and very little systemic delivery to the liver and the spleen.

Previously, this optimized LPN formulation (i.e., 15% L_5N_{12} and an L_5N_{12}:siRNA ratio of 15:1) has been demonstrated to mediate dose-dependent TNF-α mRNA silencing in vitro, and to delay arthritis progression upon intra-articular administration in a murine experimental arthritis model [6]. Enabling size-modulation of LPNs by using microfluidics opens up new avenues for investigating the effect of size on the therapeutic efficacy of LPN-assisted gene therapy in various animal disease models.

4. Conclusion

In this study, we present an alternative method to fabricate a microfluidic set up for size-controlled nanoparticle production, and we demonstrate production of 70, 110, and 220 nm LPN formulations applying the same formulation parameters. The resulting LPNs are uniform and show high siRNA loading, and they can be efficiently radiolabeled for preclinical imaging. The use of TE-microfluidic chips allows for operations in harsh chemical environments that are limited for traditional materials available for design prototyping (e.g., PDMS). The use of thiol-ene polymers effectively eliminates solvent-induced material deterioration and allows for prolonged operation in both the academic laboratory production, but also for upscaling. Moreover, we found comparable pulmonary clearance patterns of the three differently sized LPN formulations following intratracheal administration with negligible liver uptake.

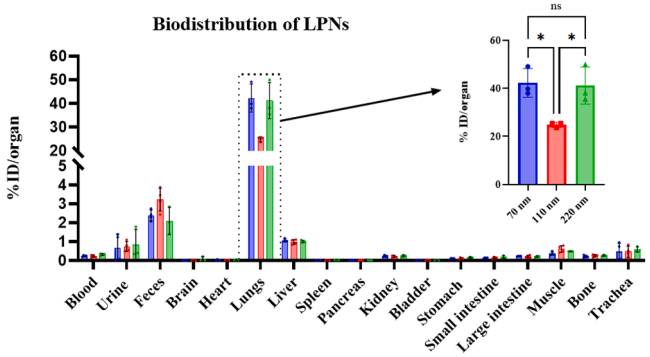

Fig. 8. Ex vivo biodistribution of the three differently sized LPN formulations evaluated at the terminal endpoint (24 h) upon analyzing the organs' radioactivity by scintillation counting. Columns represent mean values ± SD ($n = 4$). Statistically significant differences are indicated: $^*p < 0.05$. Colour code: Blue: 70 nm LPNs, red: 110 nm LPNs, green: 220 nm LPNs. (For interpretation of the references to colour in this figure legend, the reader is referred to the web version of this article.)

CRediT authorship contribution statement

Abishek Wadhwa: Conceptualization, Formal analysis, Methodology, Investigation, Funding acquisition, Writing – original draft. **Thomas R. Bobak:** Conceptualization, Formal analysis, Methodology, Investigation, Writing – original draft. **Lennart Bohrmann:** Conceptualization, Formal analysis, Investigation, Writing – original draft. **Reka Geczy:** Methodology, Investigation, Writing – review & editing. **Sathiya Sekar:** Formal analysis, Methodology, Writing – original draft. **Gowtham Sathyanarayanan:** Methodology, Investigation. **Jörg P. Kutter:** Conceptualization, Resources. **Henrik Franzyk:** Conceptualization, Resources, Writing – review & editing. **Camilla Foged:** Conceptualization, Methodology, Project administration, Funding acquisition, Supervision, Writing – review & editing. **Katayoun Saatchi:** Conceptualization, Supervision, Validation, Writing – review & editing. **Urs O. Häfeli:** Conceptualization, Methodology, Project administration, Funding acquisition, Resources, Validation, Supervision, Writing – review & editing.

Declaration of Competing Interest

Authors declare that they have no conflict of interest.

Acknowledgements

We acknowledge the financial support from the Lundbeck Foundation (Grant number 2014-4176). We also appreciate the support from Innovative Medicines Initiative Joint Undertaking under grant agreement no. 115363 resources which are composed of financial contribution from the European Union's Seventh Framework Programme (FP7/2007-2013) and EFPIA companies' in kind contribution. This project has received funding from the European Union's Seventh Framework Programme for research, technological development and demonstration under grant agreement No. 600207. We moreover acknowledge the DRA/Lundbeck Foundation Scholarship Programme 2020/2021 (R355-2020-949). We thank Abhijeet Girish Lokras and Akash Chakravarty for synthesizing L_5N_{12}. The authors would like to express their outermost gratitude towards Maryam Osooly for the assistance in the SPECT/CT imaging and ex vivo biodistribution. Katayoun Saatchi acknowledges the generous support of BWXT Isotope Technology Group for the supply of ^{111}In. We gratefully acknowledge the UBC Bioimaging Facility (RRID: SCR_021304) and Dr. Naoji Yubuki for their assistance with the cryo-TEM images.

Supplementary materials

Supplementary material associated with this article can be found, in the online version, at doi:10.1016/j.onano.2023.100180.

References

[1] T.C. Roberts, R. Langer, M.J.A. Wood, Advances in oligonucleotide drug delivery, Nat. Rev. Drug Discov. 19 (2020) 673–694, https://doi.org/10.1038/s41573-020-0075-7.
[2] P.R. Cullis, M.J. Hope, Lipid nanoparticle systems for enabling gene therapies, Mol. Ther. 25 (2017) 1467–1475, https://doi.org/10.1016/j.ymthe.2017.03.013.
[3] L. Zhang, J.M. Chan, F.X. Gu, J.-W. Rhee, A.Z. Wang, A.F. Radovic-Moreno, et al., Self-assembled lipid−polymer hybrid nanoparticles: a robust drug delivery platform, ACS Nano 2 (2008) 1696–1702, https://doi.org/10.1021/nn800275r.
[4] K. Thanki, X. Zeng, S. Justesen, S. Tejlmann, E. Falkenberg, E. Van Driessche, et al., Engineering of small interfering RNA-loaded lipidoid-poly(DL-lactic-co-glycolic acid) hybrid nanoparticles for highly efficient and safe gene silencing: a quality by design-based approach, Eur. J. Pharm. Biopharm. 120 (2017) 22–33, https://doi.org/10.1016/j.ejpb.2017.07.014.
[5] A.M. de Groot, K. Thanki, M. Gangloff, E. Falkenberg, X. Zeng, D.C.J. van Bijnen, et al., Immunogenicity testing of lipidoids in vitro and in silico: modulating lipidoid-mediated TLR4 activation by nanoparticle design, Mol. Ther. Nucleic Acids 11 (2018) 159–169, https://doi.org/10.1016/j.omtn.2018.02.003.
[6] M.A.A. Jansen, L.H. Klausen, K. Thanki, J. Lyngsø, J. Skov Pedersen, H. Franzyk, et al., Lipidoid-polymer hybrid nanoparticles loaded with TNF siRNA suppress inflammation after intra-articular administration in a murine experimental arthritis model, Eur. J. Pharm. Biopharm. 142 (2019) 38–48, https://doi.org/10.1016/j.ejpb.2019.06.009.
[7] K.T. Love, K.P. Mahon, C.G. Levins, K.A. Whitehead, W. Querbes, J.R. Dorkin, et al., Lipid-like materials for low-dose, in vivo gene silencing, Proc. Natl. Acad. Sci. 107 (2010) 1864–1869, https://doi.org/10.1073/pnas.0910603106.
[8] W. Yan, W. Chen, L. Huang, Reactive oxygen species play a central role in the activity of cationic liposome based cancer vaccine, J. Control Release 130 (2008) 22–28, https://doi.org/10.1016/j.jconrel.2008.05.005.
[9] Y. Aramaki, S. Takano, S. Tsuchiya, Induction of apoptosis in macrophages by cationic liposomes, FEBS Lett. 460 (1999) 472–476, https://doi.org/10.1016/S0014-5793(99)01386-1.
[10] A. Aljabbari, A.G. Lokras, J.J.K. Kirkensgaard, T. Rades, H. Franzyk, A. Thakur, et al., Elucidating the nanostructure of small interfering RNA-loaded lipidoid-polymer hybrid nanoparticles, J. Colloid Interface Sci. 633 (2023) 907–922, https://doi.org/10.1016/j.jcis.2022.11.141.
[11] K. Thanki, D. van Eetvelde, A. Geyer, J. Fraire, R. Hendrix, H. Van Eygen, et al., Mechanistic profiling of the release kinetics of siRNA from lipidoid-polymer hybrid nanoparticles in vitro and in vivo after pulmonary administration, J. Control Release 310 (2019) 82–93, https://doi.org/10.1016/j.jconrel.2019.08.004.
[12] K. Thanki, X. Zeng, C. Foged, Preparation, characterization, and in vitro evaluation of lipidoid–polymer hybrid nanoparticles for siRNA delivery to the cytosol, Methods Mol. Biol. 1943 (2019) 141–152, https://doi.org/10.1007/978-1-4939-9092-4_9.
[13] Y. Xu, A. Thakur, Y. Zhang, C. Foged, Inhaled RNA therapeutics for obstructive airway diseases: recent advances and future prospects, Pharmaceutics 13 (2021), https://doi.org/10.3390/pharmaceutics13020177.
[14] M.J. Ernsting, M. Murakami, A. Roy, S.-D. Li, Factors controlling the pharmacokinetics, biodistribution and intratumoral penetration of nanoparticles, J. Control Release 172 (2013) 782–794, https://doi.org/10.1016/j.jconrel.2013.09.013.
[15] F. Alexis, E. Pridgen, L.K. Molnar, O.C Farokhzad, Factors affecting the clearance and biodistribution of polymeric nanoparticles, Mol. Pharm. 5 (2008) 505–515, https://doi.org/10.1021/mp800051m.

[16] R.A. Petros, J.M. DeSimone, Strategies in the design of nanoparticles for therapeutic applications, Nat. Rev. Drug Discov. 9 (2010) 615–627, https://doi.org/10.1038/nrd2591.
[17] M. Peruzynska, K. Cendrowski, M. Barylak, D. Roginska, M. Tarnowski, M. Tkacz, et al., Study on size effect of the silica nanospheres with solid core and mesoporous shell on cellular uptake, Biomed. Mater. 10 (2015) 65012, https://doi.org/10.1088/1748-6041/10/6/065012.
[18] F. Lu, S. Wu, Y. Hung, C. Mou, Size effect on cell uptake in well-suspended, uniform mesoporous silica nanoparticles, Small 5 (2009) 1408–1413, https://doi.org/10.1002/smll.200900005.
[19] M. Zhu, G. Nie, H. Meng, T. Xia, A. Nel, Y. Zhao, Physicochemical properties determine nanomaterial cellular uptake, transport, and fate, Acc. Chem. Res. 46 (2013) 622–631, https://doi.org/10.1021/ar300031y.
[20] M. Maeki, N. Kimura, Y. Sato, H. Harashima, M. Tokeshi, Advances in microfluidics for lipid nanoparticles and extracellular vesicles and applications in drug delivery systems, Adv. Drug Deliv. Rev. 128 (2018) 84–100, https://doi.org/10.1016/j.addr.2018.03.008.
[21] Y. Sato, Y. Note, M. Maeki, N. Kaji, Y. Baba, M. Tokeshi, et al., Elucidation of the physicochemical properties and potency of siRNA-loaded small-sized lipid nanoparticles for siRNA delivery, J. Control Release 229 (2016) 48–57, https://doi.org/10.1016/j.jconrel.2016.03.019.
[22] N.M. Belliveau, J. Huft, P.J.C. Lin, S. Chen, A.K.K. Leung, T.J. Leaver, et al., Microfluidic synthesis of highly potent limit-size lipid nanoparticles for in vivo delivery of siRNA, Mol. Ther. Nucleic Acids 1 (2012) e37, https://doi.org/10.1038/mtna.2012.28.
[23] Y. Li, R.J. Lee, X. Huang, Y. Li, B. Lv, T. Wang, et al., Single-step microfluidic synthesis of transferrin-conjugated lipid nanoparticles for siRNA delivery, Nanomedicine 13 (2016) 371–381, https://doi.org/10.1016/j.nano.2016.09.014.
[24] Y. Kim, B. Lee Chung, M. Ma, W.J.M. Mulder, Z.A. Fayad, O.C. Farokhzad, et al., Mass production and size control of lipid–polymer hybrid nanoparticles through controlled microvortices, Nano Lett. 12 (2012) 3587–3591, https://doi.org/10.1021/nl301253v.
[25] Q. Feng, L. Zhang, C. Liu, X. Li, G. Hu, J. Sun, et al., Microfluidic based high throughput synthesis of lipid-polymer hybrid nanoparticles with tunable diameters, Biomicrofluidics 9 (2015) 52604, https://doi.org/10.1063/1.4922957.
[26] A. Bokare, A. Takami, J.H. Kim, A. Dong, A. Chen, R. Valerio, et al., Herringbone-patterned 3D-printed devices as alternatives to microfluidics for reproducible production of lipid polymer hybrid nanoparticles, ACS Omega 4 (2019) 4650–4657, https://doi.org/10.1021/acsomega.9b00128.
[27] L. Zhang, Q. Feng, J. Wang, J. Sun, X. Shi, X. Jiang, Microfluidic Synthesis of Rigid Nanovesicles For Hydrophilic Reagents Delivery, 54, Angew Chemie (International Ed), 2015, pp. 3952–3956, https://doi.org/10.1002/anie.201500096.
[28] Y. Li, X. Huang, R.J. Lee, Y. Qi, K. Wang, F. Hao, et al., Synthesis of polymer-lipid nanoparticles by microfluidic focusing for siRNA delivery, Molecules 21 (2016) 1314, https://doi.org/10.3390/molecules21101314.
[29] J.B. Edel, R. Fortt, J.C. deMello, A.J deMello, Microfluidic routes to the controlled production of nanoparticles, Chem Commun (Camb) (2002) 1136–1137.
[30] A. Budhian, S.J. Siegel, K.I. Winey, Haloperidol-loaded PLGA nanoparticles: systematic study of particle size and drug content, Int. J. Pharm. 336 (2007) 367–375, https://doi.org/10.1016/j.ijpharm.2006.11.061.
[31] M.P. Wolf, G.B. Salieb-Beugelaar, P. Hunziker, PDMS with designer functionalities—Properties, modifications strategies, and applications, Prog. Polym. Sci. 83 (2018) 97–134, https://doi.org/10.1016/j.progpolymsci.2018.06.001.
[32] D. Sticker, R. Geczy, U.O. Häfeli, J.P. Kutter, Thiol-ene based polymers as versatile materials for microfluidic devices for life sciences applications, ACS Appl. Mater. Interfaces 12 (2020) 10080–10095, https://doi.org/10.1021/acsami.9b22050.
[33] R. Geczy, M. Agnoletti, M.F. Hansen, J.P. Kutter, K. Saatchi, U.O. Häfeli, Microfluidic approaches for the production of monodisperse, superparamagnetic microspheres in the low micrometer size range, J. Magn. Magn. Mater. 471 (2019) 286–293, https://doi.org/10.1016/j.jmmm.2018.09.091.
[34] Hansson J., Karlsson J.M., Carlborg C.F., van der Wijngaart W., Haraldsson T. Low gas permeable and non-absorbent rubbery OSTE+ for pneumatic microvalves, 2014, p. 987. 10.1109/MEMSYS.2014.6765809.
[35] T.M. Sikanen, J.P. Lafleur, M.-E. Moilanen, G. Zhuang, T.G. Jensen, J.P. Kutter, Fabrication and bonding of thiol-ene-based microfluidic devices, J. Micromech. Microeng. 23 (2013) 37002–37007, https://doi.org/10.1088/0960-1317/23/3/037002.
[36] A. Lokras, A. Thakur, A. Wadhwa, K. Thanki, H. Franzyk, C. Foged, Optimizing the intracellular delivery of therapeutic anti-inflammatory TNF-α siRNA to activated macrophages using lipidoid-polymer hybrid nanoparticles, Front. Bioeng. Biotechnol. 8 (2021) 14, https://doi.org/10.3389/fbioe.2020.601155.
[37] Y. Xu, E. Parra-Ortiz, F. Wan, O. Cañadas, B. Garcia-Alvarez, A. Thakur, et al., Insights into the mechanisms of interaction between inhalable lipid-polymer hybrid nanoparticles and pulmonary surfactant, J. Colloid Interface Sci. 633 (2022) 511–525, https://doi.org/10.1016/j.jcis.2022.11.059.
[38] A.M. Loening, S.S. Gambhir, AMIDE: a free software tool for multimodality medical image analysis, Mol. Imaging 2 (2003) 131–137, https://doi.org/10.1162/153535003322556877.
[39] R.R. Gidde, P.M. Pawar, B.P. Ronge, N.D. Misal, R.B. Kapurkar, A.K. Parkhe, Evaluation of the mixing performance in a planar passive micromixer with circular and square mixing chambers, Microsyst. Technol. Sens., Actuators, Syst. Integr. 24 (2018) 2599–2610, https://doi.org/10.1007/s00542-017-3686-0.
[40] X. Zhu, Y. Xu, L.M. Solis, W. Tao, L. Wang, C. Behrens, et al., Long-circulating siRNA nanoparticles for validating Prohibitin1-targeted non-small cell lung cancer treatment, Proc. Natl. Acad. Sci. USA 112 (2015) 7779–7784, https://doi.org/10.1073/pnas.1505629112.
[41] H.K. Makadia, S.J. Siegel, Poly lactic-co-glycolic acid (PLGA) as biodegradable controlled drug delivery carrier, Polymers (Basel) 3 (2011) 1377–1397, https://doi.org/10.3390/polym3031377.
[42] N. Quintero, E.E. Stashenko, J.L. Fuentes, The influence of organic solvents on estimates of genotoxicity and antigenotoxicity in the SOS chromotest, Genet. Mol. Biol. 35 (2012) 503–514, https://doi.org/10.1590/S1415-47572012000300018.
[43] J. Galvao, B. Davis, M. Tilley, E. Normando, M.R. Duchen, M.F. Cordeiro, Unexpected low-dose toxicity of the universal solvent DMSO, FASEB J. 28 (2014) 1317–1330, https://doi.org/10.1096/fj.13-235440.
[44] M. Oivanen, S. Kuusela, H. Lönnberg, Kinetics and mechanisms for the cleavage and isomerization of the phosphodiester bonds of RNA by Brønsted acids and bases, Chem. Rev. 98 (1998) 961–990, https://doi.org/10.1021/cr960425x.
[45] D.G. Anderson, A. Akinc, A. Zumbuehl, M. Goldberg, E.S. Leshchiner, V. Busini, et al., A combinatorial library of lipid-like materials for delivery of RNAi therapeutics, Nat. Biotechnol. 26 (2008) 561–569, https://doi.org/10.1038/nbt1402.
[46] L. Wu, L.P. Wu, J. Wu, J. Sun, Z. He, C. Rodríguez-Rodríguez, et al., Poly(lactide-co-glycolide) nanoparticles mediate sustained gene silencing and improved biocompatibility of siRNA delivery systems in mouse lungs after pulmonary administration, ACS Appl. Mater. Interfaces 13 (2021) 3722–3737, https://doi.org/10.1021/acsami.0c21259.
[47] J. Kirch, M. Guenther, N. Doshi, U.F. Schaefer, M. Schneider, S. Mitragotri, et al., Mucociliary clearance of micro- and nanoparticles is independent of size, shape and charge—An ex vivo and in silico approach, J. Control Release 159 (2012) 128–134, https://doi.org/10.1016/j.jconrel.2011.12.015.
[48] Z. Huang, Y. Huang, W. Wang, F. Fu, W. Wang, S. Dang, et al., Relationship between particle size and lung retention time of intact solid lipid nanoparticle suspensions after pulmonary delivery, J. Control Release Off. J. Control Release Soc. 325 (2020) 206–222, https://doi.org/10.1016/j.jconrel.2020.06.004.
[49] Q. Liu, J. Guan, L. Qin, X. Zhang, S. Mao, Physicochemical properties affecting the fate of nanoparticles in pulmonary drug delivery, Drug Discov. Today 25 (2020) 150–159.
[50] J. Kim, A. Jozic, Y. Lin, Y. Eygeris, E. Bloom, X. Tan, et al., Engineering lipid nanoparticles for enhanced intracellular delivery of mRNA through inhalation, ACS Nano (2022), https://doi.org/10.1021/acsnano.2c05647.
[51] M. Agnoletti, C. Rodríguez-Rodríguez, S.N. Kłodzińska, T.V.F. Esposito, K. Saatchi, H. Mørck Nielsen, et al., Monosized polymeric microspheres designed for passive lung targeting: biodistribution and pharmacokinetics after intravenous administration, ACS Nano 14 (2020) 6693–6706, https://doi.org/10.1021/acsnano.9b09773.